Osmotic Compression of Anisotropic Proteins: Interaction Properties and Associated Structures in Wheat Gliadin Dispersions

ARTICLE *in* THE JOURNAL OF PHYSICAL CHEMISTRY B · APRIL 2015

Impact Factor: 3.3 · DOI: 10.1021/acs.jpcb.5b01673 · Source: PubMed

4 AUTHORS, INCLUDING:

Adeline Boire
French National Institute for Agricultural Rese…
5 PUBLICATIONS **27** CITATIONS
SEE PROFILE

Paul Menut
Montpellier SupAgro
25 PUBLICATIONS **329** CITATIONS
SEE PROFILE

Christian Sanchez
Université de Montpellier
75 PUBLICATIONS **2,717** CITATIONS
SEE PROFILE

THE JOURNAL OF PHYSICAL CHEMISTRY B

Article

pubs.acs.org/JPCB

Osmotic Compression of Anisotropic Proteins: Interaction Properties and Associated Structures in Wheat Gliadin Dispersions

Adeline Boire,† Paul Menut,* Marie-Hélène Morel, and Christian Sanchez

UMR IATE, Université de Montpellier, Montpellier SupAgro, INRA, CIRAD, 2, Place Viala, 34060 Montpellier Cedex 1, France

ABSTRACT: In this Article, we investigated the interaction properties of wheat gliadins, properties that are at the basis of their functionality in wheat grain and in food matrixes. We established the equation of state of our isolate by osmotic compression and characterized the concentration-induced structural transitions, from the secondary structure of proteins to the rheological properties. We evidenced three thermodynamical regimes corresponding to several structuring regimes. First, for $\Phi < 0.03$, gliadins behave as repulsive colloids, with a positive second virial coefficient, arising presumably from their surface charge density and/or their steric repulsion. No intermolecular interaction was detected by FT-IR, suggesting that proteins form a stable dispersion. In the second regime, the system becomes more easily compressible, i.e., less repulsive and/or more attractive. It is associated with the disappearance of β-sheet intramolecular structures of the proteins in favor of random coils/α-helix and intermolecular β-sheet interactions. This coincides with the appearance of elasticity and the increase of the apparent viscosity. Finally, in the last regime, for $\Phi > 0.16$, FT-IR spectra show that proteins are strongly interacting via intermolecular interactions. A correlation peak develops in SAXS, revealing a global order in the dispersion. Interestingly, the osmotic pressure applied to extract the solvent is higher than expected from a hard-sphere-like protein and we highlighted a liquid-like state at very high concentration (>450 g L^{-1}) which is in contrast with most proteins that form gel or glass at such concentration. In the discussion, we questioned the existence of supramolecular assemblies and the role of the solvation that would lead to this specific behavior.

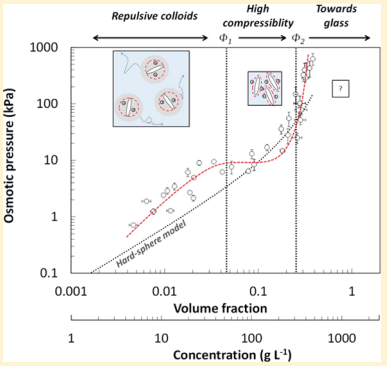

1. INTRODUCTION

Wheat storage proteins are known to form under hydration and shear a viscoelastic matrix called gluten. It confers to wheat the properties to be processed into a large range of food products with widely contrasted textures, e.g., leavened bread, pasta, and pastries.[1,2] While the biochemical composition of wheat gluten has been widely studied, its structuring mechanisms remain speculative.[3−5] Among wheat storage proteins, two main biochemical groups have been defined: gliadins, monomeric proteins with a molecular weight ranging from 30 to 70 kg mol^{-1} and pHi ranging from 5 to 8, and glutenins, polymeric proteins with a molecular weight that can reach several millions of Da.[1,6,7] In a previous work, we have shown on a wheat protein isolate that gliadins below 45 kg mol^{-1} behave as colloidal particles whereas proteins above 45 kg mol^{-1} behave as neutral linear polymers.[8] In the present work, we aim to characterize in more detail the interaction properties of the same protein isolate from diluted to concentrated system using osmotic compression experiments.

Osmotic compression was used to determine the equation of state, osmotic pressure vs volume fraction, of our isolate. The equation of state for an ideal solution, i.e., a solution in which the solute molecules are too far apart to interact, is described by the van't Hoff equation

$$\Pi V = nRT \tag{1}$$

with Π being the osmotic pressure, n the number of moles, R the ideal gas constant, and T the temperature. By analogy to the ideal gas law, the osmotic pressure depends only on temperature and on the number of molecules per unit volume. For a hard sphere dispersion, the equation of state takes into account an additional parameter: the contribution of steric repulsion at high volume fraction. It is described by the Carnahan−Starling equation:[9]

$$\frac{\Pi}{nRT} = \frac{1 + \Phi + \Phi^2 - \Phi^3}{(1 - \Phi)^3} \tag{2}$$

Such a model has been successfully applied to several protein systems such as casein micelles.[10] However, the equation of state of colloidal or protein dispersions can be more complex, as it can display long/short-range repulsion/attraction in addition to hard core repulsion. For example, short-range attractive forces can induce gel transition, resulting in a plateau on the equation of state.[11]

Here, we investigate the osmotic compression of wheat gliadins at 20 °C. Gliadins deviate from the hard-sphere model in several aspects based on the existing data on their structural and biochemical properties. First, they are not spherical, and have been instead approximate to prolate ellipsoids with aspect ratios ranging from 5 to 30 depending on the solvent and technics used.[12−15] Anisotropy leads to higher excluded volume, increasing at low concentration the effective volume fraction and subsequently steric repulsion.[16] Another deviation

Received: February 18, 2015
Revised: March 31, 2015
Published: April 3, 2015

DOI: 10.1021/acs.jpcb.5b01673
J. Phys. Chem. B 2015, 119, 5412−5421

from the hard-sphere model originates from the presence of attractive/repulsive patches on the protein surface. This depends on the amino-acid composition of the protein, on the solvent condition, and on the corresponding protein conformation. According to their amino-acid compositions, gliadins have a lower charge density than other globular proteins like ovalbumin or myoglobin.[17] This may promote poor electrostatic repulsion even though it depends on the ionic strength. In addition, high surface hydrophocity was found by both hydrophobic interaction chromatography and interfacial properties at the air−water interface.[18,19]

How these properties at a protein scale drive the colligative properties of protein phases in dilute and condensed systems remains unclear. It is in particular of interest to understand how these interactions drive gliadin properties both in gluten and during seed development. This knowledge is fundamental to control their implementation in food matrixes for controlled mechanical or nutritional properties. Also, it could help to better understand the specificities of wheat protein assemblies as compared to other cereals that have very similar protein composition but cannot generate a dense viscoelastic matrix.[7]

We led a thermodynamical approach to probe these interaction properties combined with a structural characterization to establish the link between their interaction properties and their structural and mechanical properties. We started from dilute gliadin dispersions at $\Phi = 0.005$ and applied an external osmotic pressure via dialysis against solutions of synthetic polymers. Once equilibrated, we determined the equation of state and we characterized the structures of the systems from the molecular to macroscopic scales using FT-IR spectroscopy, small angle X-ray scattering, and rheology. This paper is organized as follows. First, we describe in the Experimental Section the biochemical properties of the proteins used in this study and the experimental methods and analytical treatments used for the characterization. Second, we present the main results and compare them with results obtained with other protein systems, when available. Finally, we discuss in the third section the structuring behavior of wheat gluten proteins in terms of three successive regimes.

2. EXPERIMENTAL SECTION

2.1. Materials. We developed a gentle procedure to extract proteins from wheat grains based on the differential solvent solubility of wheat flour proteins as described in our previous work.[8] From this procedure, we obtained a wheat protein isolate composed mainly of gliadins (92.0 ± 1.7%). We defined five groups based on their molecular weight (MW) and their biochemical classification:

- group 1, glutenins with MWs > 70 kg mol^{-1}
- group 2, ω-gliadins with 55 kg mol^{-1} < MWs < 70 kg mol^{-1}
- group 3, ω-gliadins with 45 kg mol^{-1} < MWs < 55 kg mol^{-1}
- group 4, α-, β-, and γ-gliadins, with 35 kg mol^{-1} < MWs < 45 kg mol^{-1}
- group 5, α-, β-, and γ-gliadins with 25 kg mol^{-1} < MWs < 35 kg mol^{-1}.

Their respective mean MW and proportions are reported in Table 1. In our previous work, we found that gliadins of groups 4 and 5 behave in dilute suspension as colloidal particles and have similar interaction properties. Using osmotic compression, we expect to probe the interaction properties of these two groups, as they represent 81 wt % of the total mixture and they have the smallest MW. Using the van't Hoff equation, we found that they should have the greatest contribution to the overall osmotic pressure of the dispersions (89.8%).

Table 1. Protein Composition of the Wheat Protein Isolate

		proportion of each group in the protein mixture	
	mean MW (kg mol^{-1})	% weight	% molar
group 1	285	8.0	2.6
group 2	57	5.7	3.4
group 3	46	5.7	4.3
group 4	35	36.2	35.8
group 5	28	44.5	54.0

2.2. Preparation of Osmotic Stress Experiments. The objective of this technique is to determine the equation of state, i.e., the osmotic pressure vs concentration relationship, of our gliadin isolate. The method used here consists of equilibrating gliadin dispersions against a surrounding bath containing a polymer solution of higher osmotic pressure.

Polyethylene glycol (PEG) with a molar mass of 20 000 Da (Sigma-Aldrich) was used as the stressing polymer. We determined the osmotic pressure of PEG 20 000 in 55% v/v ethanol/water mixture, 0.5 mM NaCl at 20 °C at several concentrations using a home-built membrane osmometer. The membrane osmometer device consists of two fluid chambers of 6 mL separated by a SpectraPor membrane (cutoff 3500 Da) hold on a porous support. The system is equipped with pressure sensors (Keller, Cambridge, U.K.) covering the range of 0.0 to 10.0 bar +/− 0.1%, a range of measurement of osmotic pressure of 0 to 1000 kPa, +/− 2 kPa. The voltage output of the transducer was recorded in 30 s intervals using Picolog Software (Picotechnology LTD, Cambridge, U.K.). Results showed that the experimental data in 55% v/v ethanol/water mixture, 0.5 mM NaCl at 20 °C were well fitted with the equation found with water at 20 °C (online data - https://www.brocku.ca/researchers/peter_rand/osmotic/osfile.html).

Freeze-dried gliadins were dissolved into 55% v/v ethanol/water solution using a magnetic stirrer to reach 10 g L^{-1}. An ethanol/water mixture is used, as wheat proteins are poorly soluble in water due to their large repeated apolar sequences.[20] Residual undissolved solids were removed by centrifugation for 10 min at 20 000g. The dispersions were then filtered on a 0.22 μm Nylon filter (Magna). Protein dispersions were then placed into a dialysis bag with a cutoff of 12 000 kDa (Spectrapore) and put into opaque containers at 20 °C with PEG 20 000 in 55% v/v ethanol solution, NaCl 0.5 mM.

Twelve PEG concentrations were tested between 0.5 and 21.0% m/v. A volume ratio of 1:20 was kept constant between the protein dispersion and the surrounding bath to ensure a constant salt concentration among all the dialysis conditions. Volumes of the systems were comprised between 0.14 and 1.8 L. For PEG concentrations above 8.0%, the dialysis bags were filled in two stages: at time 0 and 3 days later because the volume of the protein dispersion was large (>50 mL). After 4 weeks, dialysis tubes were removed from the bath of PEG. The protein concentrations were determined by UV absorption spectroscopy, using a specific absorbance coefficient ($A_{280\ nm}$, 1 cm) of 0.570 L g^{-1} cm^{-1} as determined experimentally. When aggregation was observed through the appearance of weak turbidity, the protein concentration was determined after

DOI: 10.1021/acs.jpcb.5b01673
J. Phys. Chem. B 2015, 119, 5412−5421

removal of the visible aggregates (which do not contribute to the osmotic pressure) by centrifugation for 10 min at 25 000*g*.

At the end of the dialysis, the concentration of PEG in the bath was determined using a method developed and based on the precipitation of PEG by iodine.[21] Twenty μL of a PEG solution with a concentration range between 0.005 and 0.3% m/v was put into a 1 mL solution of iodine (0.1 mM) and vortexed during 10 s. The absorbance of the solution at 600 nm was then read by UV−visible spectroscopy 30 s after the injection of PEG solution. The absorbance must be measured at a fixed time because the absorbance is time dependent. The concentration of PEG, in g L^{-1}, is linear with absorbance and follows eq 3.

$$A(600\text{ nm},\ 1\text{ cm}) = 0.5853\ [\text{PEG}] \tag{3}$$

After dialysis, the structure of protein dispersions was determined within 2 weeks. The 12 dialysis conditions were repeated three times with 3 weeks in between.

In the following sections, protein concentrations will be expressed in volume fraction Φ to compare our results with classic models such as hard-sphere. The volume fraction Φ is defined as the fraction of the total volume V that is filled by N spherical proteins, each of radius r:

$$\Phi = \frac{4}{3}\pi r^3 \frac{N}{V} \tag{4}$$

The way of defining and determining the radius of a particle is the subject of controversy even on an experimental model system such as PMMA particle.[22] Here, this is even more difficult, as (i) gliadins are anisotropic objects and (ii) proteins radius can change depending on physical-chemical conditions.[23] We chose here to convert protein concentration into volume fraction Φ using the partial specific volume ν = 0.76 mL g^{-1} of crude gliadin:[24]

$$\Phi = \nu \times c \tag{5}$$

The resulting Φ does therefore not rely on any hypothesis on the protein hydration layer nor on excluded volume effects due to anisotropy, both effects being part of our discussion. We also used this definition to compute the Carnahan−Starling equation, eq 2.

2.3. Fourier Tranform Infrared Spectroscopy (FT-IR). *2.3.1. Measurements.* FT-IR experiments were performed in total attenuated reflection mode (ATR-FT-IR) at 25 °C in a Tensor 27 Bruker spectrometer (Bruker, Karlsruhe, Germany) equipped with an ATR cell (GladiATR, Pike Technology, Cottonwood, Madison, WI, USA) and a MCT (mercury−cadmium−telluride) detector cooled with liquid N2 (Bruker, Karlsruhe, Germany). The diaphragm was set to 3 mm. The scanning rate was 20 kHz. A total of 32 scans were used for both the reference and the sample between 4000 and 800 cm^{-1} at 2 cm^{-1} resolution.

The reference was first recorded at 25 °C on air; then, spectra of 20 μL protein dispersions were recorded at 25 °C. The spectrum of 20 μL of 55% water−ethanol mixture was recorded at 25 °C for manual background subtraction during the data treatment. Three repeats were carried out for each sample. In total, 12 concentrations were analyzed per dialysis.

2.3.2. Data Treatment. The following treatments were carried out using OPUS software (Bruker, Karlsruhe, Germany). First, raw absorbance spectra were smoothed using a 13-point Savitsky−Golay smoothing function and cut between 1710 and 1485 cm^{-1}. Baseline correction using two points was applied to spectra, that were further cut between 1710 and 1585 cm^{-1}.

Spectra were corrected from the solvent background by subtraction. Spectra were centered and normalized according to

$$X_{x,y} = \frac{S_{x,y} - a\nu_x}{\text{SD}_x} \tag{6}$$

where $X_{x,y}$ represents the centered and normalized spectra, $S_{x,y}$ is the absorbance value of spectra x and wavenumber y, $a\nu_x$ indicates the average absorbance of spectrum x, and SD_x stands for the standard deviation of the absorbance of spectrum x. We used the resulting spectra to determine differential spectra by subtracting the first spectrum from all the other ones.

2.3.3. Generalized Two-Dimensional (2D) Correlation Analysis. Centered and normalized FT-IR spectra were treated by generalized 2D correlation. Analysis was done using the 2Dshige v1.3 software kindly provided by Dr. Shigeaki Morita (formerly at Kwansei-Gakuin University).

2.4. Small Angle X-ray Scattering (SAXS). SAXS experiments were performed using an in-house setup at the Laboratoire Charles Coulomb, "Réseau X et gamma", Université de Montpellier, France. A high brightness low power X-ray tube, coupled with aspheric multilayer optics (GeniX3D from Xenocs), was employed. It delivers an ultralow divergent beam (0.5 mrad). Scatterless slits were used to give a clean 0.8 mm beam diameter (35 Mphotons/s) at the sample (wavelength λ = 1.5418 Å). We worked in a transmission configuration, and scattered intensity was measured by a Schneider 2D image plate detector prototype, at a distance of 1.9 m from the sample. All intensities were corrected by transmission, and the empty cell contribution was subtracted.

2.5. Rheological Measurements. *2.5.1. Protein Dispersion for Φ < 0.02.* A capillary viscometer (Cannon-Ubbelohde, Cannon Inst. Co., tube reference number: Tyn 51813) was used to measure the viscosities of protein dispersions for Φ < 0.02. The capillary was cleaned successively with deionized water and ethanol 96% v/v and rinsed with acetone, and finally dried with compressed air before use. The temperature was controlled at 20.0 ± 0.1 °C. Three viscosities were measured at each concentration. Capillary Newtonian viscosities were determined at ±1%.

2.5.2. Protein Dispersion for Φ > 0.02. All rheological measurements were performed at 20.0 ± 0.1 °C using a Peltier temperature-controlled plate.

Rheological properties of wheat gliadin dispersions for Φ > 0.02 were measured using a stress-controlled AR 2000ex rheometer (TA Instruments, USA) equipped with a 20 mm and 4° cone plate geometry.

We used a solvent trap and saturated the environment with the solvent vapor to prevent evaporation. Prior to any rheological measurements, a preshear at 1 s^{-1} was performed for 30 s to eliminate sample stress history. A dynamical measurement at 0.1 Hz, 3% of strain was performed for 10 min to check that the sample was at equilibrium after the preshear.

We determined the apparent viscosity of protein dispersions successively with three different methods. First, a steady shear measurement was conducted to determine apparent viscosity over shear rates ranging from 0.02 to 200 s^{-1}, with 10 points per decade. Apparent viscosity was determined on the Newtonian plateau at a small shear rate.

Then, a small-amplitude oscillatory shear experiment was conducted over a frequency range of 0.05−60 Hz, yielding the

DOI: 10.1021/acs.jpcb.5b01673
J. Phys. Chem. B 2015, 119, 5412−5421

shear storage G' and loss G'' moduli at 3% of strain. A strain–sweep experiment was conducted from 0.1 to 100% at 0.1 Hz to ensure that measurements were in the linear viscoelastic range. The complex viscosity η^* was calculated with eq 7

$$\eta^* = \frac{1}{J^*(\omega) \times \omega} \tag{7}$$

with J^* being the complex compliance and ω the frequency.

Finally, a creep test was performed to determine the zero-shear viscosity by applying a shear stress of 0.05 Pa for 10 min. The (near-) zero-shear viscosity was determined as the inverse of the slope of the compliance curve when a constant slope is reached, usually tending to 10 min.

Measurements of the apparent, complex, and zero-shear viscosity gave some similar values: we calculated an average viscosity (giving an equivalent weight to each of them), which is used for the discussion. Our data are therefore an average of three measurements repeated three times for each condition, and in the graph, the error bars give an indication of the variability between methods.

3. RESULTS

3.1. Equation of State of Wheat Gliadin Isolate. We determined the equation of state of the wheat gliadin isolate by studying the effect of osmotic pressure on their volume fraction at equilibrium, as plotted in Figure 1. It reveals the existence of two volume fractions Φ_1 and Φ_2 at about 0.03 and 0.2, separating three main regimes.

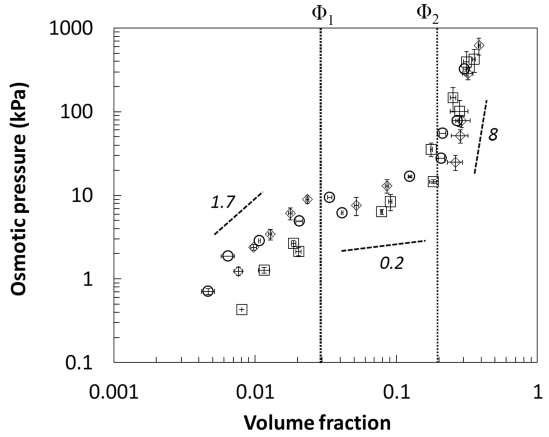

Figure 1. Osmotic pressure of wheat gliadin dispersions at 20 °C of three repeats (○, □, ◇) after 4 weeks of equilibration. Dashed lines are guides for the eye corresponding to a power law with exponents of 1.7, 0.2, and 8. Dotted lines separate three regimes with the characteristic volume fraction Φ_1 and Φ_2.

In the first regime, for $\Phi < \Phi_1$, the relationship osmotic pressure vs protein volume fraction can be described by a power law of about 1.7. Although we observed a significant variability of the experimental data between the three replicates, we found that the experimental osmotic pressure deviates from the exponent of 1 predicted by van't Hoff theory. Such deviation can be explained by the effect of attractive or repulsive interactions within the system. We used a second-order virial equation of state to describe this deviation, as depicted in eq 8.

$$\frac{\Pi}{RT} = \frac{c}{M} + B_2 c^2 \tag{8}$$

The second virial coefficient B_2 accounts for the particle–particle interaction. A positive value of B_2 indicates that repulsive interactions are occurring, whereas a negative value means dominant attractions in the system. Using eq 8, we obtained a positive value comprised between 2.0 and 4.7×10^{-3} mol mL g^{-2}, indicative of globally repulsive interactions.

In the second regime, for $\Phi_1 < \Phi < \Phi_2$, a discontinuity in the equation of state is observed. The osmotic pressure is either constant or only slightly increasing. The system becomes therefore more easily compressible, i.e., less repulsive and/or more attractive.

A third regime occurs for $\Phi > \Phi_2$, in which the osmotic pressure rises much faster, approximately as the eighth power of volume fraction.

3.2. Structural Characterization at a Macroscopic Scale. Increasing volume fractions are associated with changes in flowing and optical properties, as illustrated in Figure 2.

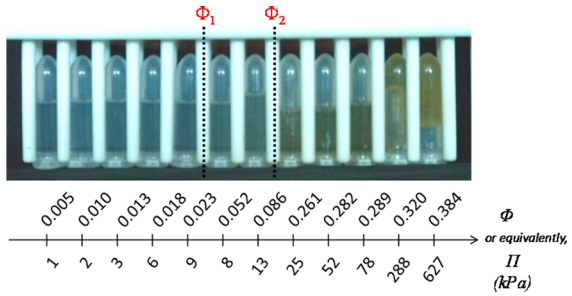

Figure 2. Tubes containing wheat gliadin dispersions with increasing volume fraction (0.005 to 0.384) obtained after 4 weeks of osmotic compression (1 kPa < Π < 627 kPa). The picture was taken 10 s after tubes overturning to show the differences in flowing behavior. Dotted lines show the position of the characteristic volume fraction identified in Figure 1.

Wheat gliadin dispersions at $\Phi < \Phi_2$ are fluid, mostly transparent with some white eye naked detectable aggregates.

At higher osmotic pressure, for $\Phi > \Phi_2$, dispersions are notably more viscous and yellowish-colored. They become visually even more viscous for $\Phi = 0.32$ and 0.38: this last dispersion still does not flow 12 h after overturning the tubes.

We investigated the effect of increasing volume fractions on the rheological properties. The values of viscosity for all the measurements are reported in Figure 3. Three power laws were used as a first approach to describe the observed behavior. It gives rise to three exponents: 1.7 for $\Phi < 0.04$, 2.3 for $0.04 < \Phi < 0.2$, and 8 for $0.2 < \Phi$. In the second regime, this value is close to 2.7, the value found for α-zein (a maize storage proteins), under acetic acid conditions.[23]

In addition, the linear viscoelastic properties of wheat gliadins have been investigated for $0.02 < \Phi$. The frequency dependence of G' and G'' is reported in Figure 4A. For clarity, the plots are vertically shifted by the factor α, as indicated in the figure. At all volume fractions, G'' is higher than G' for frequencies comprised between 0.01 and 10 s^{-1}, indicating a liquid-like character. This is supported by the proportionality to ω^2 and ω of G' and G'', respectively, for $\Phi < 0.29$. For $\Phi > 0.29$, G' and G'' exhibit a weaker frequency dependence with exponents of 1 and 0.85, respectively. For these samples, the absolute values of G' and G'' rise much faster as a function of Φ with an exponent of the order of 20 (Figure 4B).

DOI: 10.1021/acs.jpcb.5b01673
J. Phys. Chem. B 2015, 119, 5412–5421

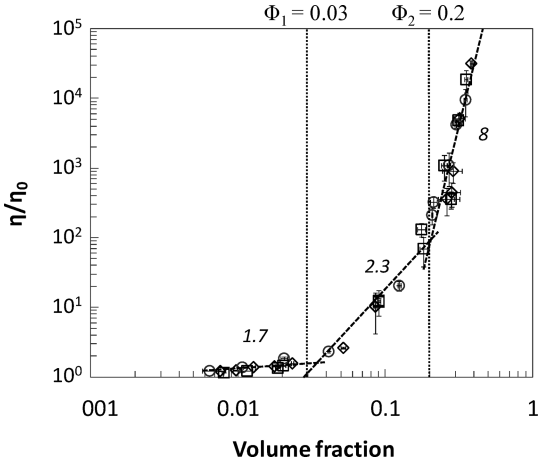

Figure 3. Volume fraction dependence of the relative viscosity of wheat gliadin dispersions at 20 °C in 55% v/v ethanol/water solution (0.5 mM NaCl). For Φ < 0.04, measurements were carried out with a capillary viscosimeter. The three different symbols (◇, ○, □) stand for the three different dialysis batches. The three dotted lines stand for power laws. The positions of Φ_1 and Φ_2 are reported on the graph.

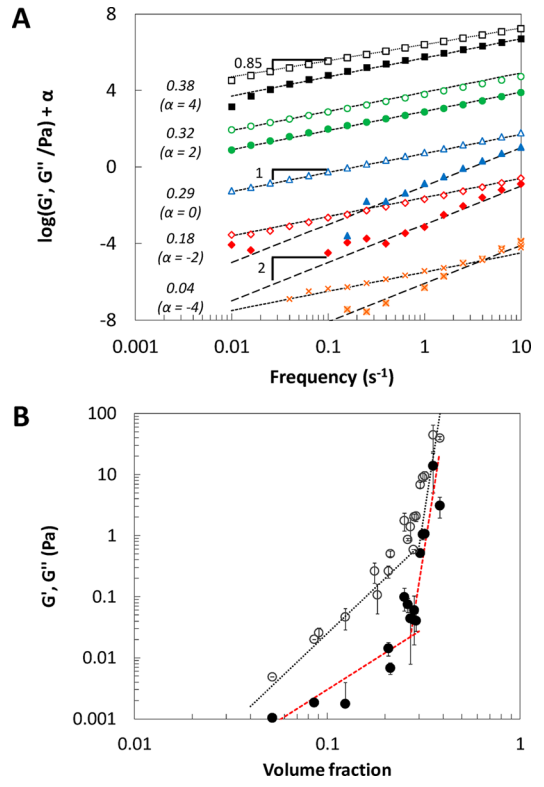

Figure 4. (A) Frequency dependence of the storage G' (filled symbols) and loss G'' (empty symbols) moduli of wheat gliadin dispersions at volume fractions of 0.04, 0.18, 0.29, 0.32, and 0.38 in 55% v/v ethanol/water solution (0.5 mM NaCl) at 20 °C. Plots are shifted vertically for clarity by the factor α indicated in brackets. Large dashed lines stand for a power law of 2, small dashed lines stand for a power law of 1, and the dotted line stands for a power law of 0.85. (B) Absolute value of storage G' (diamonds) and loss G'' (circle) moduli as a function of volume fraction (at 20 °C, 0.1 Hz, and 3% of strain) with the associated power law exponents.

3.3. Structural Characterization at a Mesoscopic Scale for Φ > 0.2. The structure of wheat gliadin dispersions was also investigated through small-angle X-ray scattering experiments (SAXS) using a lab setup. Data have been recorded for 0.21 < Φ < 0.38 to get enough signals.

Figure 5 shows the experimental scattered intensity normalized by the concentration. When Φ ≤ 0.28, the

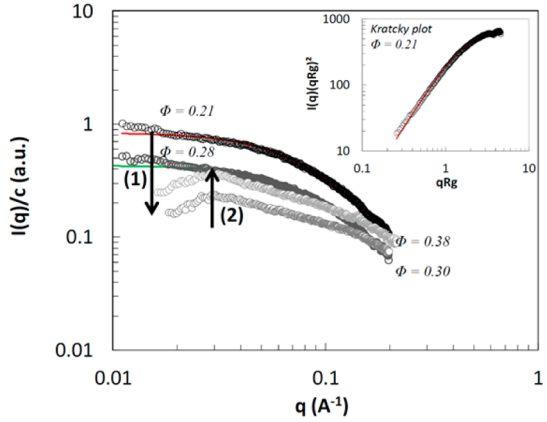

Figure 5. Scattering intensity normalized by concentration $I(q)/c$ of wheat gliadin dispersions (1) from Φ = 0.21 (top) to 0.28 (intermediate) to 0.3 (bottom) and (2) from 0.3 to 0.38 g L^{-1} obtained by SAXS at 20 °C in 55% v/v water−ethanol mixture. Solid lines for Φ = 0.21 (red) and 0.3 (green) are the theoretical triaxial ellipsoid form factors. Inset: Kratky plot of form factor with the theoretical Kratky plot of triaxial ellipsoid (red line).

scattered intensity only contained a contribution from the form factor (no structure factor peak), which can be fitted as a triaxial ellipsoid (see the Kratky plot for Φ = 0.21 in the inset of Figure 5). The axes of the modeled triaxial ellipsoid are similar for Φ = 0.21 and 0.28: we found a = 1.8 nm for two minor axes and L = 8.4 nm for the major axis. The gyration radius calculated from the Guinier region gives a value of 2.5 nm. A similar aspect ratio, around 5−5.5, was found in a dilute dispersion in 70% v/v ethanol−water mixture[14] but with larger axis lengths (L = 15.1 nm and a = 3.2 nm).

For Φ = 0.3, a structure factor appeared, revealing an order in the dispersion. Its position at about 0.3 nm^{-1} gives a correlation length Λ ($=2\pi/q$) of about 20 nm. We observed that this transition is associated with a yet-unexplained nonmonotonous evolution of the scattered intensity with increasing volume fraction.

3.4. Structural Changes at a Molecular Scale. *3.4.1. General Effect of Increasing Volume Fraction on the Secondary Structure.* Secondary structures of proteins were investigated using Fourier transform infrared spectroscopy (FT-IR) and analyzed between 1600 and 1700 cm^{-1}. This area, called the amide I band, is sensitive to variations in molecular geometry and hydrogen bonding patterns of proteins, and dominated by signals of the backbone CO vibrations. Infrared spectra for volume fractions comprised between 0.005 and 0.38 at 25 °C in the amide I region are shown in Figure 6. They display a broad band centered around 1650−1655 cm^{-1}, which is typical of predominantly α-helix/random coil proteins with a significant shoulder at 1630 cm^{-1}, characteristic of β-sheet structures.[25] The second derivative of the spectra allows identifying more precisely five main frequencies:

- at 1650−1655 cm^{-1}, classically assigned to random coil and/or α-helix structures
- at 1614 cm^{-1}. Besides it is usually considered difficult to assign precisely this frequency, it has been attributed to

DOI: 10.1021/acs.jpcb.5b01673
J. Phys. Chem. B 2015, 119, 5412−5421

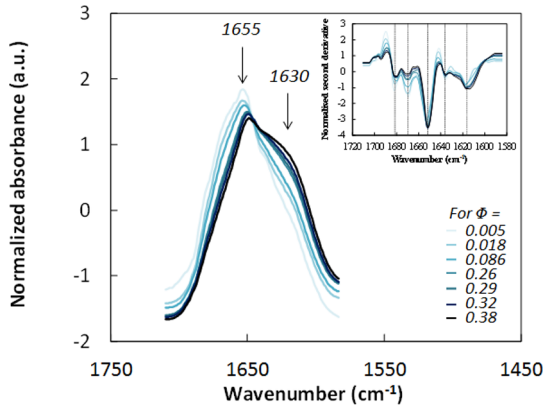

Figure 6. Normalized absorbance in the amide I region of wheat protein dispersions at a temperature of 25 °C for protein volume fractions comprised between 0.005 and 0.38. Inset: derivative of the amide I band of wheat protein dispersions for each volume fraction. Each spectrum is the average of three measurements.

strong hydrogen bonding.[26] It can be mainly related to intermolecular β-sheets, side chain vibration, or extended β-strands.

- at 1636 cm^{-1}, attributed to intramolecular β-sheets
- at 1670 cm^{-1}, ascribed to β-turn absorptions. The repetitive domains of wheat proteins rich in proline residues are supposed to contribute to these turns.[25,27,28]
- at 1682 cm^{-1}, attributed to β-sheets or β-turns[27,28]

Increasing Φ induces a decrease in vibration of a broad band at 1650−1690 cm^{-1} corresponding to (i) random coils and α-helix (1640−1660 cm^{-1}), (ii) turns/bends (1660−1685 cm^{-1}), and (iii) a high-frequency component of intramolecular β-sheets (1685−1690 cm^{-1}). In parallel, vibrations in the range 1600−1640 cm^{-1} are increased by increasing concentration.

3.4.2. Several Regimes of Structuring. Protein structural changes can be discriminated with differential spectra which are calculated by subtracting the first centered and normalized spectrum (Φ = 0.005) from all the other ones. The absorbance changes observed while increasing protein concentration are both concentration and wavelength dependent. This is illustrated for seven wavelengths in Figure 7. At both extremities of the frequency range, at 1610 cm^{-1} and above 1670 cm^{-1}, the absorbance increases or decreases monotonously with concentration. For intermediate wavelength, we observed a two-step evolution, in which an initial increase (decrease) of the absorbance is followed by its decrease (increase). This is the case, for example, at 1630 and 1640 cm^{-1} where the absorbance first decreases and then increases. The opposite trend is observed at 1650 cm^{-1}. In each case, the turnaround occurs at a similar volume fraction, $\Phi_{FT\text{-}IR}$ = 0.12, represented as a dashed line in Figure 7. It should be noted that, for Φ < 0.02, the absorbance is not significantly affected by the increase in concentration, which can be due either to an absence of effect or a too weak signal.

We used a 2D-correlation analysis to study in more detail correlations between FT-IR signal evolutions observed while increasing protein concentration. Two correlation maps are generated through this analysis: a 2D synchronous map and a 2D asynchronous map. The synchronous spectrum represents the coincidental changes of spectral intensities measured at two frequencies ν_1 and ν_2. It displays vibration wavenumbers that are significantly coupled and whose changes are in-phase at

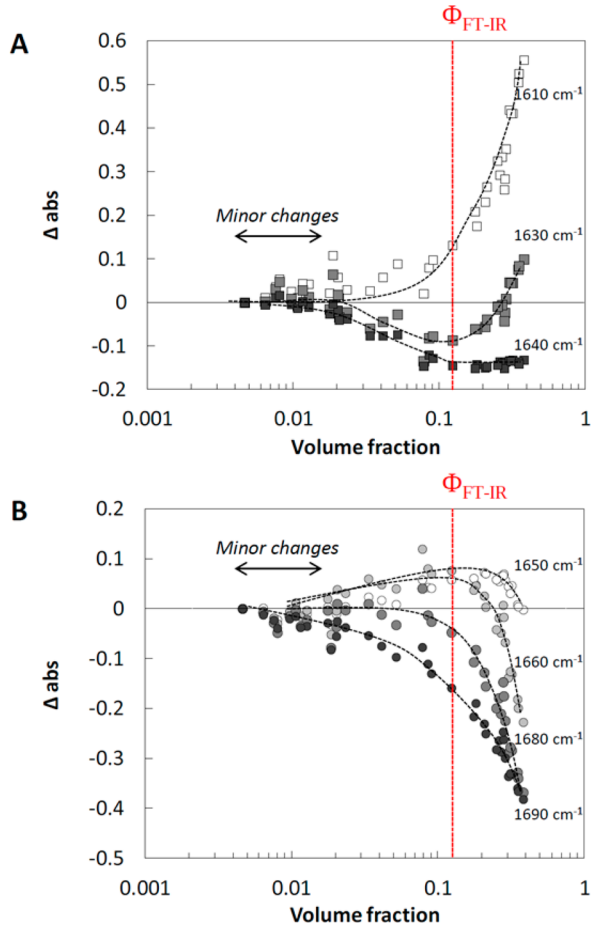

Figure 7. Concentration dependence of the absorbance change at frequencies 1610, 1630, and 1640 cm^{-1} (A) and at 1650, 1660, 1680, and 1690 cm^{-1} (B) for the 34 concentrations tested. Dashed lines stand for a characteristic volume fraction separating two domains as explained in the text.

similar rates while increasing Φ.[29] The asynchronous spectrum instead represents the sequential or successive changes of spectral intensities measured at ν_1 and ν_2. It displays vibration wavenumbers that are significantly decoupled and whose changes are out-of-phase at different rates while increasing Φ. In addition, an argument map is generated. It represents the global phase angle description of the 2D correlation analysis. It is expressed as $\Theta = \tan^{-1}(\Psi/\Omega)$, with Ψ and Ω being the asynchronous and synchronous spectra, respectively.[29]

2D correlation analysis is strictly applicable in the case of monotonous evolution of intensities. We therefore split the analysis in two regimes: below and above $\Phi_{FT\text{-}IR}$, as reported in Figure 8. For both regimes, the intensity scale of the synchronous map is more than 10 times higher than the one of the asynchronous map, leading to a global phase angle Θ close to 0, as shown by the widely white argument map. As synchronous events were largely dominant, we only analyze the 2D synchronous map in the following section.

Regime 1: Φ < 0.12. The diagonal displays the wavenumber whose intensity is changed as compared to the average spectra of the data set. Two major correlation peaks are found at 1640 cm^{-1} (β-sheet) and at 1655 cm^{-1} (random coils/α-helices), and two minor correlation peaks are found at 1614 cm^{-1} (strong interaction regions/intermolecular β-sheets) and 1690 cm^{-1} (β-sheet intramolecular). The autopeak at 1655 cm^{-1} is broad with

DOI: 10.1021/acs.jpcb.5b01673
J. Phys. Chem. B 2015, 119, 5412−5421

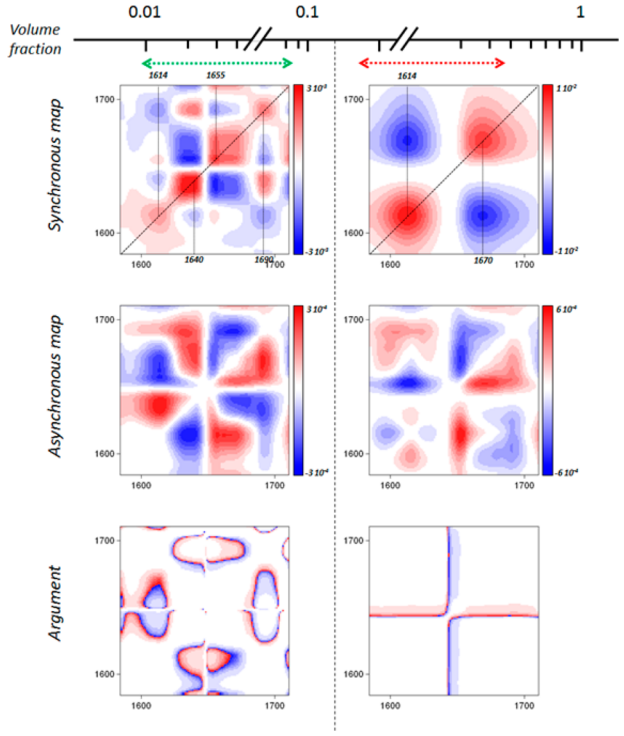

Figure 8. 2D-correlation analysis of FT-IR spectra of a wheat gliadin dispersions obtained at 25 °C, between 1580 and 1710 cm^{-1}, for volume fractions comprised between 0.005 and 0.38. Two separate analyses were made, one for $\Phi < 0.12$ and one for $\Phi > 0.12$.

low resolution, suggesting that additional peaks are buried underneath[30] between 1655 and 1670 cm^{-1} (β-turn). The off-diagonal allows determining the wavenumbers that are synchronous. There is a positive cross-peak at 1614 and 1655 cm^{-1}, meaning that their intensity changes in the same direction. In contrast, cross-peaks at 1614 and 1655 cm^{-1} are negatively correlated to cross-peaks at 1640 and 1690 cm^{-1}, meaning that their intensity changes in the opposite direction. This is in good agreement with Figure 7 where absorbance increases at 1610 and 1650 cm^{-1} and decreases at 1640 and 1690 cm^{-1}. It indicates that strong interactions between proteins associated with the formation of intermolecular β-sheets, as well as formation of β-turn and random coils/α-helices are increasing, to the detriment of intramolecular β-sheets.

Regime 2: $\Phi > 0.12$. During this second regime, two major correlation peaks are found at 1614 cm^{-1} (strong interaction regions/intermolecular β-sheets) and 1670 cm^{-1} (β-turns) which are negatively correlated. Absolute intensities are increasing at 1614 cm^{-1} and decreasing at 1670 cm^{-1} (Figure 7), which indicates that the content of intermolecular β-sheets and interactions between proteins are increasing to the detriment of β-turns.

4. DISCUSSION

The results clearly showed that the concentration-dependent structuring of wheat gliadin can be split into three regimes. This discussion aims to provide a better understanding of the interaction properties in each of them, by correlating thermodynamical results, i.e., osmotic pressure curve, and the multiscale structural changes.

4.1. Regime 1: $\Phi < 0.03$. The dilute regime corresponds to wheat gliadin dispersions equilibrated at pressures below 10 kPa. It is characterized by a positive second virial coefficient, suggesting that proteins are mostly repulsive. This is coherent with minor or no changes in FT-IR spectra, meaning the absence of conformational changes and intermolecular interactions. Repulsion can arise from steric or electrostatic effects, which we now discuss.

The shape of gliadins has been approximated to prolate ellipsoids. Under dilute conditions, the excluded volume of such anisotropic particles can be modeled by a sphere encompassing the particle. This leads to a higher excluded volume than for a spherical particle. The steric repulsion is therefore higher than expected due to the anisotropy. Considering proteins as ellipsoids is however still an approximation, and it has been shown by numerical simulations that their local surface roughness should also be included in order to estimate their second virial coefficient. Such an exercise conducted on various types of ellipsoid-like proteins demonstrates that, in general, their excluded volume value is about 7 times the molecular volume.[31]

Repulsion can also arise from electrostatic repulsion. The surface charges of a protein strongly affect the local concentration of dissolved ions, leading to the formation of an electrical double layer. The Debye length κ characterizes the thickness of this layer. The longer the Debye length, the longer ranged the electrostatic interactions will be. Debye length is inversely proportional to the square root of ionic strength and is described as follows

$$\kappa^{-1} = \sqrt{\frac{\varepsilon_r \varepsilon_0 k_B T}{2 N_A e^2 I}} \tag{9}$$

with I being the ionic strength of the solution, ε_0 the permittivity of free space, ε_r the dielectric constant, k_B the Boltzmann constant, T the absolute temperature, N_A the Avogadro number, and e the elementary charge. In 55% v/v ethanol−water solution and 0.5 mM NaCl, the Debye length is 10.8 nm. This value is large in comparison to the average interparticle distance $\langle D \rangle$, which is estimated through eq 10.[16]

$$\frac{\langle D \rangle_{\text{isotropic}}}{L} = \left(\frac{\Phi^*}{\Phi_{\text{sphere}}} \right)^{1/3} \tag{10}$$

where L is the major axis length of the particle and Φ_{sphere} the volume fraction of spheres encompassing the anisotrope gliadin. The latter is defined using the following equation:

$$\Phi_{\text{sphere}} = \Phi_{\text{particle}} \frac{\pi / 6 L^3}{V} \tag{11}$$

This equation only applies for $\Phi_{\text{sphere}} < \Phi^*$, with Φ^* being the critical volume fraction, which corresponds to the volume fraction for which the equivalent spheres fill the whole volume, $\Phi^* = 1$ and $\Phi_{\text{gliadin}} = 0.045$. In the first regime, the average interparticle distance decreases from about 8.8 nm for $\Phi_{\text{gliadin}} = 0.005$ to 4.8 nm for $\Phi_{\text{gliadin}} = 0.03$. As those average interparticle distances are always shorter than the Debye length, electrostatic repulsion cannot be neglected. Taken together, the steric repulsion and the electrostatic repulsion should be responsible for the overall repulsion observed in the first regime.

4.2. Regime 2: $0.03 < \Phi < 0.16$. For the second regime in osmotic pressure, the system becomes more easily compressible. If the localization of the lower limit of this regime is quite

DOI: 10.1021/acs.jpcb.5b01673
J. Phys. Chem. B 2015, 119, 5412−5421

clear (around Φ = 0.03), the upper limit is questionable. Indeed, different values were found through osmotic compression (Φ = 0.2, see Figure 1), viscosity (Φ = 0.2, see Figure 3), and FT-IR (Φ = 0.12, see Figure 7) measurements. Considering that only few data were obtained in the range 0.12−0.2, the discrepancy might not be significant, and we will consider from now that the upper limit of this regime is in the range 0.16 ± 0.04.

This regime corresponds to a progressive disorganization of the internal structure of the protein, evidenced by a decrease in intramolecular β-sheet content and the appearance of intermolecular interactions. The absence of a structure factor in SAXS scattering profiles by the end of the regime, however, suggests that gliadins are still in isolated form. The pseudoplateau observed in the equation of state is the thermodynamical signature of this regime. A plateau could be associated with a sol−gel transition;[11,32] however, here the rheological characterization of the suspension clearly showed that it remains liquid. Instead, we have currently identified two main hypotheses.

First, the plateau could result from an anisotropic ordering of the proteins. As detailed previously, the critical volume fraction Φ^* at which Φ_{sphere} fills the whole volume corresponds to a volume fraction of gliadin of 0.045, in the range of the second regime. A decrease of the excluded volume associated with ordering may therefore explain the higher compressibility of the system. However, it should be noted that no birefringence was observed on the plateau.

Our second hypothesis is related to internal structural rearrangement of the proteins that may increase their density and/or change their interaction properties. As proteins are flexible, they may locally rearrange to withstand the unfavorable positions induced by electrostatic repulsion. Changes in their conformation are suggested by FT-IR. In addition, we obtained, by SAXS, smaller dimensions at high concentration compared to the ones obtained under diluted conditions,[14] suggesting denser proteins as observed on zein.[23] Compaction via conformational changes has also been suggested for BSA, leading to a lower net charge and to changes in the range and the strength of interaction.[33] Such structural transition of the protein conformation may also decrease the repulsion of the proteins and/or increase their density and lead to the higher compressibility observed.

4.3. Regime 3: 0.12/0.2 < Φ. Major changes were detected in the last osmotic regime, namely, (i) a sharp increase in viscosity for Φ > 0.2, (ii) changes in ω-dependence of G' and G'' for Φ > 0.3, (iii) appearance of a correlation peak in SAXS for Φ > 0.3, and (iv) a drastic increase of the vibration at 1614 cm^{-1} indicative of strong interprotein interactions. The third regime is associated with significant changes in the dynamical properties of the dispersions. The frequency dependence of both G' and G'' is less marked, but their absolute values strongly increase with volume fraction: for example, G' increases by 3 decades between Φ = 0.3 and Φ = 0.38, at 0.1 Hz.

In hard sphere systems approaching the glass transition, G' also increases drastically when approaching its close packing fraction to reach a plateau at higher volume fraction. It has been shown in emulsion and casein dispersion that, at this plateau, G' and the osmotic pressure are of the same order of magnitude.[34,35] Here, G' is well below the osmotic pressure, suggesting that the system behaves as a viscoelastic liquid going toward glass transition. This behavior would be in that respect similar to the one recently observed in α-crystallin solutions, for which glass transition was observed for a protein concentration of 340 g L^{-1},[36] and illustrates the specific property of wheat gliadins, which here remain liquid up to 500 g L^{-1} (or Φ = 0.38).

In the third regime, the behavior of gliadin deviates from Carnahan−Starling (Figure 9). Even though the model gives

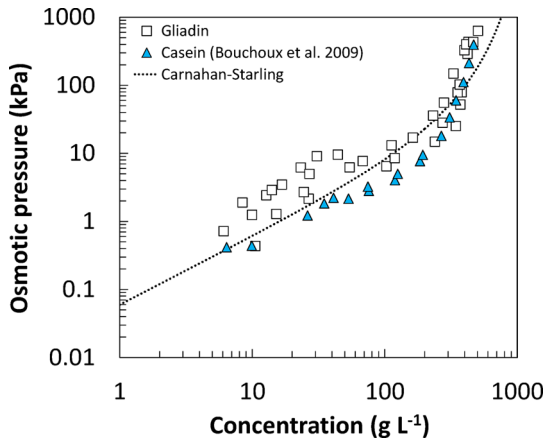

Figure 9. Osmotic compression by dialysis of gliadins (pH 7, white square) and casein micelles (pH 6.7, blue triangle)[10] and Carnahan−Starling prediction for gliadins.

the right order of magnitude, it fails in describing the main features of our experimental data: mainly a higher slope for the first regime and a divergence in regime 3 that may be underestimated, at first sight, because of the log−log scale. However, the behavior of gliadins is surprisingly similar to that of casein micelles, a supramolecular assembly as illustrated in Figure 9.[10] Above 10 kPa, the osmotic compression induces the "deswelling" of casein micelles. A high energy is required to compress the micelle and extract the water trapped inside. The strong resistance to concentration of gliadins may suggest by analogy the formation of associated structures for which organization is capable of supporting compressive osmotic stress. However, unlike casein micelles, gliadins do not gel in this "deswelling" process, and remain in a liquid-like state despite the increase of viscoelasticity, suggesting the transient or liquid-like nature of those structures. Many questions are raised by these observations about the mesoscopic structure of the system at such a high concentration. Formation of dynamic clusters in protein solutions has been observed in lysozyme suspension, suggested by the presence of a q-independent peak position in SAXS studies,[37,38] at lower concentration than the one at which we observe a peak here.

The analogy with casein micelles, which could be seen as sponges, could also indicate that strong solvation forces play a role in the strong resistance to concentration of gliadins. This is, however, less obvious if we use β-sheet complexes for analogy instead of casein micelles. In such a system, a similar β-sheet transition is observed upon increasing hydrostatic pressure but such a transition is associated with a greater volume of hydrophobic cavities, leading to a lower hydration.[39] This analogy would rather indicate that the solvation of gliadins decreases with increasing β-sheet content. However, unlike most β-sheet complexes, gliadins contain short β-sheet stretches flanked by looser extended chains.[28] The presence of these disordered regions is thought to play a role in the

DOI: 10.1021/acs.jpcb.5b01673
J. Phys. Chem. B 2015, 119, 5412−5421

solvation of wheat proteins.[28,40] Combining the model of β-sheet complexes together with the model of intrinsically disordered proteins may help us to better understand the solvation issue of wheat proteins and know whether or not it plays a role in the intriguing behavior we observed in this regime. One could imagine studying model polypeptides, with or without a disordered sequence, upon osmotic compression and see how disordered sequences affect the behavior at high concentration. Such an approach on model polypeptides has been successfully used to understand the helix−coil transition in poly(glutamicacid) upon osmotic compression.[41]

Clarifying the role of the supramolecular assembly and of the hydration of individual proteins in condensed systems could help in understanding the protein behavior in real systems, in the seed and in the food products in which they are present at a large concentration. In wheat seed, proteins are localized in spherical protein bodies of about 10 μm in diameter in which their concentration could approach 350 g L^{-1}, assuming that protein bodies and seed water content are equal. The ability of wheat proteins to maintain a liquid-like state at such concentrations might be essential both for the optimal filling of protein bodies as well as for protein efficient extraction at the time of germination. Their rheological properties may also be essential for dough development to promote extension of the protein bodies under shear and stickiness between proteins, conditions required for the formation of a protein percolating network in a dough in which dispersed proteins account for only 9−12% of the total mass of the flour.

5. CONCLUSION

In the present work, we established the experimental relationship osmotic pressure vs volume fraction for wheat gliadins and investigated the structural properties of the dispersions at several scales. On the basis of this approach, several regimes of concentration are evidenced. During the first regime, for $\Phi < 0.03$, protein behaves like repulsive colloids, with a positive second virial coefficient certainly arising from their surface charge density and their steric repulsion. No intermolecular interaction was detected by FT-IR, suggesting that proteins form a stable dispersion. In the second regime, the system becomes more easily compressible, i.e., less repulsive and/or more attractive. This is associated with the disappearance of the β-sheet intramolecular structures of the proteins in favor of random coils/α-helix and intermolecular attractive interactions. It coincides with the appearance of elasticity and the increase of the apparent viscosity. Finally, in the last regime, for $\Phi > 0.16$, FT-IR spectra show that proteins are strongly interacting via intermolecular interactions. A correlation peak develops in SAXS, revealing an emerging supramolecular organization in the dispersion. The pressure to apply to extract the solvent is much higher than observed on hard-sphere-like proteins, suggesting a "deswelling" of the system. The drastic increase of the elasticity in the last regime suggests that the glass transition is approaching. Within the range of volume fraction investigated, below 0.4, i.e., concentrations below 500 g L^{-1}, the protein dispersions are viscoelastic with liquid-like character. This may be indicative of a peculiar supramolecular organization that can withstand such high pressure and/or a specific role of hydration.

AUTHOR INFORMATION

Corresponding Author

*Fax: +334 67 63 54 09. Phone: +334 99 61 30 18. E-mail: menutp@supagro.inra.fr.

Present Address

[†]FOM Institute AMOLF, 1098XG Amsterdam, The Netherlands.

Notes

The authors declare no competing financial interest.

ACKNOWLEDGMENTS

We would like to thank Philippe Dieudonne-George from Laboratoire Charles Coulomb for performing the SAXS experiments. We also gratefully acknowledge our colleagues Yannick Hallez, Martine Meireles, and Patrice Bacchin from LGC Toulouse and Denis Renard from INRA Nantes for fruitful discussions.

REFERENCES

(1) Shewry, P. R.; Halford, N. G. Cereal seed storage proteins: structures, properties and role in grain utilization. *J. Exp. Bot.* **2002**, *53*, 947−958.

(2) Wrigley, C. W. Biopolymers - Giant proteins with flour power. *Nature* **1996**, *381*, 738−739.

(3) Hamer, R. J.; van Vliet, T.; Lefebvre, J. Letter to the Editor. *J. Cereal Sci.* **2005**, *42*, 344−345.

(4) MacRitchie, F. Letter to the Editor. *J. Cereal Sci.* **2007**, *46*, 96−97.

(5) van Vliet, T.; Hamer, R. J. Letter to the Editor. *J. Cereal Sci.* **2007**, *46*, 98−99.

(6) Shewry, P. R.; Field, J. M.; Faulks, A. J.; Parmar, S.; Miflin, B. J.; Dietler, M. D.; Lew, E. J. L.; Kasarda, D. D. The purification and n-terminal amino-acid sequence-analysis of the high molecular-weight gluten polypeptides of wheat. *Biochim. Biophys. Acta* **1984**, *788*, 23−34.

(7) Shewry, P. R.; Tatham, A. S. The prolamin storage proteins of cereal seeds - structure and evolution. *Biochem. J.* **1990**, *267*, 1−12.

(8) Boire, A.; Menut, P.; Morel, M.-H.; Sanchez, C. Phase behavior of a wheat protein isolate. *Soft Matter* **2013**, *9*, 11417−11426.

(9) Carnahan, N. F.; Starling, K. E. Equation of State for Nonattracting Rigid Spheres. *J. Chem. Phys.* **1969**, *51*, 635−636.

(10) Bouchoux, A.; Cayemitte, P.-E.; Jardin, J.; Gesan-Guiziou, G.; Cabane, B. Casein Micelle Dispersions under Osmotic Stress. *Biophys. J.* **2009**, *96*, 693−706.

(11) Chik, J. K.; Parsegian, V. A. The entropically favored osmotic "compression" of sickle cell hemoglobin gels. *Biopolymers* **2001**, *59*, 120−124.

(12) Lamm, O.; Polson, A. The determination of diffusion constants of proteins by a refractometric method. *Biochem. J.* **1936**, *30*, 528−541.

(13) Entrikin, P. P. The dielectric behavior of solutions of the protein gliadin. *J. Am. Chem. Soc.* **1941**, *63*, 2127−2131.

(14) Thomson, N. H.; Miles, M. J.; Popineau, Y.; Harries, J.; Shewry, P.; Tatham, A. S. Small angle X-ray scattering of wheat seed-storage proteins: α-, γ- and ω-gliadins and the high molecular weight (HMW) subunits of glutenin. *Biochim. Biophys. Acta* **1999**, *1430*, 359−366.

(15) Ang, S.; Kogulanathan, J.; Morris, G. A.; Kok, M. S.; Shewry, P. R.; Tatham, A. S.; Adams, G. G.; Rowe, A. J.; Harding, S. E. Structure and heterogeneity of gliadin: a hydrodynamic evaluation. *Eur. Biophys. J. Biophys. Lett.* **2010**, *39*, 255−261.

(16) Baravian, C.; Michot, L. J.; Paineau, E.; Bihannic, I.; Davidson, P.; Imperor-Clerc, M.; Belamie, E.; Levitz, P. An effective geometrical approach to the structure of colloidal suspensions of very anisometric particles. *Europhys. Lett.* **2010**, *90*, 36005.

(17) Macritchie, F. Physicochemical Properties of Wheat Proteins in Relation to Functionality. *Adv. Food Nutr. Res.* **1992**, *36*, 1−87.

(18) Popineau, Y.; Godon, B. Surface hydrophobicity of gliadin components. *Cereal Chem.* **1982**, *59*, 55−62.

DOI: 10.1021/acs.jpcb.5b01673
J. Phys. Chem. B 2015, 119, 5412−5421

(19) Popineau, Y.; Pineau, F. Investigation of surface hydrophobicities of purified gliadins by hydrophobic interaction chromatography, reversed-phase high-performance liquid-chromatography and apolar ligand-binding. *J. Cereal Sci.* **1987**, *5*, 215−231.
(20) Osborne, T. B. *The proteins of the wheat kernel*; Carnegie Institution of Washington: Washington, DC, 1907.
(21) Francois, M.; Deneve, R. Determination of polyethylene glycols by precipitation with iodine. *Talanta* **1985**, *32*, 491−494.
(22) Poon, W. C. K.; Weeks, E. R.; Royall, C. P. On measuring colloidal volume fractions. *Soft Matter* **2012**, *8*, 21−30.
(23) Li, Y.; Xia, Q.; Shi, K.; Huang, Q. Scaling Behaviors of alpha-Zein in Acetic Acid Solutions. *J. Phys. Chem. B* **2011**, *115*, 9695−9702.
(24) Zhang, Z.; Scanlon, M. G. Solvent effects on the molecular structures of crude gliadins as revealed by density and ultrasound velocity measurements. *J. Cereal Sci.* **2011**, *54*, 181−186.
(25) Pezolet, M.; Bonenfant, S.; Dousseau, F.; Popineau, Y. Conformation of wheat gluten proteins - comparison between functional and solution states as determined by infrared-spectroscopy. *FEBS Lett.* **1992**, *299*, 247−250.
(26) Georget, D. M. R.; Belton, P. S. Effects of Temperature and Water Content on the Secondary Structure of Wheat Gluten Studied by FTIR Spectroscopy. *Biomacromolecules* **2006**, *7*, 469−475.
(27) Mangavel, C.; Barbot, J.; Popineau, Y.; Gueguen, J. Evolution of wheat gliadins conformation during film formation: A Fourier transform infrared study. *J. Agric. Food Chem.* **2001**, *49*, 867−872.
(28) Wellner, N.; Belton, P. S.; Tatham, A. S. Fourier transform IR spectroscopic study of hydration-induced structure changes in the solid state of omega-gliadins. *Biochem. J.* **1996**, *319*, 741−747.
(29) Noda, I. 2-dimensional infrared (2D IR) spectroscopy - theory and applications. *Appl. Spectrosc.* **1990**, *44*, 550−561.
(30) Filosa, A.; Wang, Y.; Ismail, A.; English, A. M. Two-dimensional infrared correlation spectroscopy as a probe of sequential events in the thermal unfolding of cytochromes c. *Biochemistry* **2001**, *40*, 8256−8263.
(31) Neal, B. L.; Lenhoff, A. M. Excluded volume contribution to the osmotic second virial coefficient for proteins. *AIChE J.* **1995**, *41*, 1010−1014.
(32) Mourchid, A.; Delville, A.; Lambard, J.; Lecolier, E.; Levitz, P. Phase-diagram of colloidal dispersions of anisotropic charged-particles - equilibrium properties, structure, and rheology of laponite suspensions. *Langmuir* **1995**, *11*, 1942−1950.
(33) Sarangapani, P. S.; Hudson, S. D.; Jones, R. L.; Douglas, J. F.; Pathak, J. A. Critical Examination of the Colloidal Particle Model of Globular Proteins. *Biophys. J.* **2015**, *108*, 724−737.
(34) Mason, T. G.; Lacasse, M. D.; Grest, G. S.; Levine, D.; Bibette, J.; Weitz, D. A. Osmotic pressure and viscoelastic shear moduli of concentrated emulsions. *Phys. Rev. E* **1997**, *56*, 3150−3166.
(35) Bouchoux, A.; Debbou, B.; Gesan-Guiziou, G.; Famelart, M. H.; Doublier, J. L.; Cabane, B. Rheology and phase behavior of dense casein micelle dispersions. *J. Chem. Phys.* **2009**, *131*, 165106.
(36) Foffi, G.; Savin, G.; Bucciarelli, S.; Dorsaz, N.; Thurston, G. M.; Stradner, A.; Schurtenberger, P. Hard sphere-like glass transition in eye lens α-Crystallin solutions. *Proc. Natl. Acad. Sci. U. S. A.* **2014**, *111*, 16748−16753.
(37) Stradner, A.; Sedgwick, H.; Cardinaux, F.; Poon, W. C. K.; Egelhaaf, S. U.; Schurtenberger, P. Equilibrium cluster formation in concentrated protein solutions and colloids. *Nature* **2004**, *432*, 492−494.
(38) Grobelny, S.; Erlkamp, M.; Möller, J.; Tolan, M.; Winter, R. Intermolecular interactions in highly concentrated protein solutions upon compression and the role of the solvent. *J. Chem. Phys.* **2014**, *141*, 22D506.
(39) Cordeiro, Y.; Kraineva, J.; Ravindra, R.; Lima, L. M. T. R.; Gomes, M. P. B.; Foguel, D.; Winter, R.; Silva, J. L. Hydration and Packing Effects on Prion Folding and β-Sheet Conversion: high pressure spectroscopy and pressure perturbation calorimetry studies. *J. Biol. Chem.* **2004**, *279*, 32354−32359.
(40) Belton, P. S.; Gil, A. M.; Grant, A.; Alberti, E.; Tatham, A. S. Proton and carbon NMR measurements of the effects of hydration on the wheat protein ω-gliadin. *Spectrochim. Acta, Part A* **1998**, *54*, 955−966.
(41) Stanley, C.; Strey, H. H. Osmotically induced Helix-Coil Transition in Poly(glutamic acid). *Biophys. J.* **2008**, *94*, 4427−4434.

DOI: 10.1021/acs.jpcb.5b01673
J. Phys. Chem. B 2015, 119, 5412−5421